coefficient $\lambda(T)$ has on heat conductivity solids and/or liquids.

The set of parameters, γ, obtained in the present paper through solving the inverse problem of heat conductivity under various conditions, allows one to establish the laws of change in the thermal characteristics of the substances. The most obvious in this respect is manifested in studying two- or three-dimensional problems. For instance, in propagating temperature waves in three-dimensional space (xyz) under laser radiation action, the gradient of the heat conductivity coefficient will be different in various directions, if the temperatures at sections $z = l_1, y = l_2$ and $x = l_3$ are not the same, i.e. $T_2 \neq T_3 \neq T_4$, where T_2, T_3 and T_4 are the temperatures at points $z = l_1, y = l_2$ and $x = l_3$, respectively. Having resolved the inverse problem for each direction independently, in this case, one will get three various laws of the parameter γ alteration, namely:

$$\gamma_z = \frac{2}{T_1 + T_2}, \quad \gamma_y = \frac{2}{T_1 + T_3}, \quad \gamma_x = \frac{2}{T_1 + T_4}.$$

In other words, along axes x, y and z, the heat flow under the laser radiation action will be different, even if the medium, a priori, was isotropic.

REFERENCES

1. Carslaw, H.S. and Jaeger, J.C., *Conduction of Heat in Solids*, Nauka Press, Moskva, pp 92-94 (1964).
2. Belyayev, N.M. and Ryadno, A.A., *Methods of Nonstationary Heat Conductivity*, High School, Moskva, pp 19-52 (1978).
3. Goldberg, M.A., *Boundary Integral Methods. Numerical and Mathematical Aspects*, WIT Press, Southampton, pp 120-175 (1998).
4. Hassanov, H.G. "New analytical methods for solving non-linear problems of heat conductivity", *Report on the 1st Inter. Conf. on Nonlinear Analysis and Nonlinear Modelling*, Fethiye, Turkey (2001).
5. Hassanov, H.G. and Aliyev, A.A. "About one inverse problem of electrothermodynamics", *J. of Oil and Gas. Transact. of Azerb. State Oil Acad.*, **3**, pp 23-26 (2001).
6. Gasanov, G.T. and Musayev, M.A. "About optical method of determination of liquids acoustic properties", *J. of Oil and Gas. Transact. of Azerb. State Oil Acad.*, **2**, pp 35-38 (1994).
7. Galich, N.E. "Turbulence generated by laser radiation in liquid", *J. of Tech. Phys.*, **50**(6), pp 1196-1199 (1980).
8. Zuyev, V.I. "Experimental investigation of non-stability of convection caused by laser radiation", *J. of Tech. Phys.*, **56**(2), pp 394-396 (1986).
9. Hassanov, G.T. and Hassanov, H.G. "Effect of high-frequency electromagnetic fields on thermodynamic properties of heavy-viscous liquids", *1st Inter. Conf. on Tech. & Phys. Prob. of Power Engrg.*, **1**, pp 345-349 (2002).

Scientia Iranica, Vol. 11, No. 4, pp 378–385

SCIENTIA IRANICA

Research Note

Mixed Mode Fracture of Concrete: An Experimental Investigation

M.T. Kazemi* **and F. Vossoughi Shahvari**[1]

In this paper, the mixed mode experimental results of 24 notched beams of concrete with various notch depths and locations are reported. The test results for conventional critical stress intensity factors and crack trajectories are demonstrated. It is noted that with the larger thickness, which results in conditions closer to plane strain, the crack path can be better predicted by linear elastic fracture mechanics criteria. The effects of applied load and specimen weight on the fracture are considered with the use of separate stress intensity factors. It is observed that the final failure angles, based on the crack path's intersection point with the beam's top side, are better predicted than the crack initiation angles, from the maximum principal stress criterion. Conventional mixed mode fracture toughness increases with an increase in the mode II to mode I stress intensity factors ratio.

INTRODUCTION

By now, fracture mechanics is universally acknowledged as a viable tool of analysis for investigation of concrete cracking and failure [1-4]. Under combined normal and shear stress states, cracks tend to fracture in both mode I (opening) and mode II (sliding) configurations, so it is important to investigate crack propagation under mixed mode loading. For mixed mode failure, the determination of the failure path and the criteria for crack instability are more complicated than in pure mode I [5].

A relatively large number of experiments concerning crack initiation and propagation in mixed mode on notched specimens have been carried out in recent years [5-12]. Swartz et al. [6] measured the average total fracture energy under mixed mode concrete fracture and concluded that mode II fracture energy is eight times larger than that of mode I.

Jenq and Shah [5] compared the theoretically predicted crack initiation angles, which are based on Linear Elastic Fracture Mechanics (LEFM), with the scatter of those measured experimentally. They concluded that all the crack initiation theories give similar results.

*. *Corresponding Author, Department of Civil Engineering, Sharif University of Technology, Tehran, I.R. Iran.*

1. *Department of Civil Engineering, Sharif University of Technology, Tehran, I.R. Iran.*

Guo et al. [10] have concluded from their experiments, using moiré interferometry that aggregate interlocking increased the crack closing stress under mixed mode loading and, hence, the load carrying capacity of concrete specimens. They have proposed that there is an additional friction generated by the interlocking force, which affected the crack closing stress versus crack opening displacement relation through an increased crack closing stress.

Recent studies by Galvez et al. [11] have also shown that in concrete specimens under mixed mode loading, the crack path can be approximated by LEFM theories. In all of the foregoing studies, the starter crack was a machined notch, which was subjected to combined loading.

The purpose of this research was to further study, experimentally, the mixed mode fracture of concrete and investigate the applicability of LEFM theories for crack propagation prediction in plain concrete.

THEORY

While under pure mode I, in homogeneous isotropic materials, crack propagation is colinear, in all other cases the propagation will be curvilinear. Thus, for general mixed mode cases, one needs a criterion that will determine both the condition for fracture initiation and the angle of incipient propagation.

If a crack is loaded in combined modes I and II, the stress components, σ_θ and $\tau_{r\theta}$ (Figure 1), near the

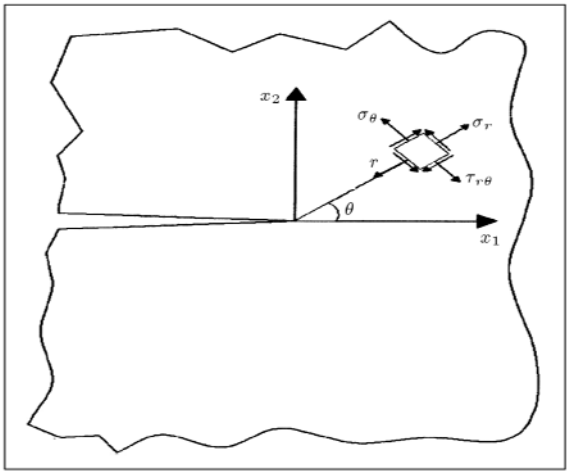

Figure 1. Axes for near crack tip field description.

tip of the crack can be obtained by adding the stresses due to mode I and mode II [2,3,13]:

$$\sigma_\theta = \frac{1}{\sqrt{2\pi r}} \cos\frac{\theta}{2}[K_I \cos^2\frac{\theta}{2} \quad \frac{3}{2}K_{II}\sin\theta], \tag{1}$$

$$\tau_{r\theta} = \frac{1}{2\sqrt{2\pi r}} \cos\frac{\theta}{2}[K_I \sin\theta + K_{II}(3\cos\theta \quad 1)], \tag{2}$$

where K_I and K_{II} are stress intensity factors for mode I and mode II, respectively. As in mode I fracture, where quasi-static crack growth requires that $K_I = K_{IC}$, for the in-plane mixed mode problems, the straight phenomenological approach consists in postulating that fracture may initiate when the values of K_I and K_{II} verify a critical condition [2,3,5,13]:

$$F(K_I, K_{II}) = 0. \tag{3}$$

To describe the kinking behavior of fracture, three most commonly used LEFM based approaches have been used. The first is a direct extension of the energetic balance condition (maximum energy release rate); the second is based on the near-tip stress distribution (maximum principal stress) and the third is the minimum strain energy density criterion. The initiation angle predicted, using any of these three models, are almost the same.

Due to simplicity, the maximum principal stress criterion is used in this paper. This criterion states that for an in-plane mixed mode, crack growth will occur perpendicular to the direction of maximum principal stress. The maximum of σ_θ (shown in Figure 1) occurs when $\tau_{r\theta}$ is zero and consequently from Equation 2, the initiation angle, θ_m, is given by:

$$tg\frac{\theta_m}{2} = \frac{K_I}{4K_{II}}\left(1 \pm \sqrt{1 + \frac{8K_{II}^2}{K_I^2}}\right). \tag{4}$$

Jenq and Shah [2,5] extended their mode I equivalent LEFM model to describe mixed mode fracture behavior. The mixed mode cohesive fracture mechanics or crack band models are required to calculate the crack propagation more accurately.

EXPERIMENTAL PROGRAM

Three point bend notched beam tests with notches at different off-set ratios, $\gamma = 2x/S$, were performed (Figure 2). The length, depth and thickness of the specimens were $L = 700$ mm, $b = 150$ mm and $t = 150$ mm, respectively. In addition, the nominal span of all the beams was $S = 600$ mm. In each position of the crack, three different notch depths were tested. Thus, the variables for all the tests were the distance between the centerline of the beam and the place of notch x and notch depth a_0.

Four different off-set ratios, ranging from 0 to 0.6 by an increment of 0.2 and each with various notch to depth ratios of 0.2 to 0.6 with 0.2 steps, were used in this study. In each crack configuration, two specimens were cast, so a total of 24 beam specimens were cast to account for different off-set ratios and notch depths. Two extra beams were cast without any notch. All of the beams were tested under a load control condition with the same loading rate. In addition, control cylinders of 152.4 mm × 304.8 mm were cast to measure the compressive strength.

MATERIALS AND SPECIMENS

Six batches of a single microconcrete mixture were used to cast the specimens. A mould with four compartments was used for the casting. The notches for specimens were produced by placing paper plates with 1.5 mm thickness and different depths in the mould before casting. The basic mix ingredients were type II Portland cement, crushed coarse aggregate, sand, water and superplasticizer. The maximum size of coarse aggregate was 12.5 mm and both coarse aggregate and sand were utilized in a Saturated Surface Dry (SSD) condition. Due to the absence of larger coarse

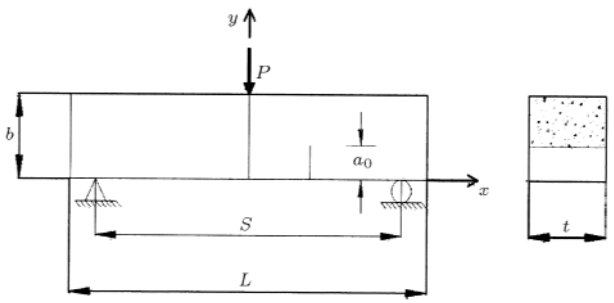

Figure 2. Schematic view of mixed mode beam specimens.

aggregate content, a superplasticizer was used and the mixing time was increased to produce uniform concrete without segregation. The weight ratios of water, coarse aggregate, sand and superplasticizer to cement were 0.45, 2, 2.5 and 0.005, respectively. Immediately after casting, wet burlaps were wrapped around the mould to avoid shrinkage cracks. After 40 hrs, all the specimens were demoulded and stored in a curing room under appropriate conditions until one day before the test. The testing age was almost 90 days for all the specimens.

CALCULATION OF STRESS INTENSITY FACTORS

Analytical solutions of the stress intensity factors are not available for the present testing configuration for off-set ratios other than zero. A finite element code was used to calculate the stress intensity factors for different configurations. Barsoum [14] demonstrated that the inverse square root singularity characteristic of LEFM could be obtained in the two-dimensional 8-nodded isoparametric element when the mid-side nodes near the crack tip are placed at the quarter point. By using this recommendation, singular elements were placed in a rosette around the crack tip. The finite element mesh pattern, given in Figure 3, was used in the numerical calculation.

The values of K_I and K_{II} were calculated from the nodal displacements near the crack tip. Usually, the stress intensity factor is expressed as $K = \sigma\sqrt{\pi a_0} f(\alpha,\gamma)$, where $\alpha = a_0/b$ and a_0 = notch depth. For the current study, since there were two stress intensity factors for mode I and mode II, i.e., K_I and K_{II}, functions f_I and f_{II} , which are dependent on α and γ, were evaluated for each crack configuration.

The stress intensity factors may be sought as:

$$K_I = \sigma_N \sqrt{b}\sqrt{\pi\alpha} f_I(\alpha,\gamma), \tag{5}$$

$$K_{II} = \tau_N \sqrt{b}\sqrt{\pi\alpha} f_{II}(\alpha,\gamma), \tag{6}$$

where:

$$\sigma_N = \frac{6M}{b^2 t(1-\alpha)^2}, \tag{7}$$

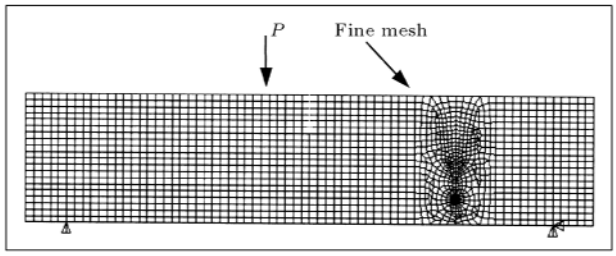

Figure 3. Finite element mesh for stress intensity factor calculation.

$$\tau_N = \frac{V}{bt(1-\alpha)}, \tag{8}$$

$f_I(\alpha,\gamma)$ and $f_{II}(\alpha,\gamma)$ are dimensionless functions, M is bending moment at distance $x = \gamma S/2$ from the centerline and V is shear force at distance x. The factor $(1-\alpha)$ was also entered to account for the net area of the beam section. By analyzing a notched beam with different crack configurations under assumed point load P and using Equations 5 to 8, dimensionless functions, f_{IP} and f_{IIP}, were calculated for required values of α and γ. The same procedure was repeated for weight load W, which resulted in values for f_{IW} and f_{IIW}. The results for f_{IP}, f_{IIP}, f_{IW} and f_{IIW} are presented in Table 1.

To have a more precise calculation of the stress intensity factors, both the effect of point load and the specimen weight should be considered. To this end, two methods may be adopted. In the first method, the combined effect of load and weight can be introduced in M and V by:

$$M = M_P + M_W, \tag{9}$$

$$V = V_P + V_W, \tag{10}$$

in which (Figure 2):

$$M_P = \frac{P}{4}(S-2x), \tag{11}$$

$$V_P = \frac{P}{2}, \tag{12}$$

$$M_W = \frac{wL}{4}(S-2x) - \frac{w}{8}(L-2x)^2, \tag{13}$$

$$V_W = wx, \tag{14}$$

Table 1. Dimensionless functions for stress intensity factors.

$\gamma = 2x/S$	$\alpha = a_0/b$	f_{IP}	f_{IW}	f_{IIP}	f_{IIW}
0.0	0.2	0.626	0.677	0.000	0.000
	0.4	0.422	0.453	0.000	0.000
	0.6	0.292	0.306	0.000	0.000
0.2	0.2	0.689	0.677	0.530	0.548
	0.4	0.459	0.453	0.671	0.699
	0.6	0.308	0.306	0.615	0.618
0.4	0.2	0.686	0.679	0.583	0.535
	0.4	0.457	0.453	0.729	0.689
	0.6	0.307	0.306	0.631	0.615
0.6	0.2	0.686	0.689	0.536	0.503
	0.4	0.457	0.455	0.693	0.669
	0.6	0.307	0.306	0.616	0.608

with $0\langle x\langle S/2$, w = weight per unit length of the beam and subscripts P and W refer to point load and weight load, respectively. Equations 5 to 8, with the appropriate values of f_{IP} and f_{IIP}, which were calculated based on the point load P, could be used to calculate K_I and K_{II}.

A better method, which was chosen in this study, is to use the superposition of stress intensity factors:

$$K_I = K_{IP} + K_{IW}, \tag{15}$$

$$K_{II} = K_{IIP} + K_{IIW}, \tag{16}$$

where K_{IP}, K_{IW}, K_{IIP} and K_{IIW} are obtained separately, based on the measured failure load and weight of the beam and have their own dimensionless functions.

RESULTS AND DISCUSSION

Critical Fracture Parameters

For the sake of brevity, to each specimen a unit code was designated. The code is a four-digit number, which follows the C (concrete) letter. The first two digits show the distance (cm) between the loading point and the initial notch, the third digit indicates the notch depth (cm) and, since for each crack configuration two specimens were cast, the last digit is added to differentiate these two, which takes the value of 1 or 2.

For the test reported here, the average compressive strength (f'_c) was 41 MPa, which is considered as normal strength concrete. Furthermore, the average specific weight for all the batches was 2300 kg/m^3. The results for measured peak loads and conventional critical stress intensity factors, which were calculated from the maximum load and the beam weight by using the initial notch depths, are listed in Table 2. It can be seen that as the distance between the center line of the specimen and the location of notch x increases, the maximum load increases too. For the present testing configuration, location of the notch (section at which the strength was reduced) and the mid-span (which is subjected to the maximum bending moment) are the two possible places that offer the least resistance to external load. To analyze the effect of weight, two parameters, r_1 and r_2, were considered; $r_1 = K_{IIP}/K_{IP}$ solely depends on the geometry and could be calculated in advance, but $r_2 = K_{IICM}/K_{ICM}$ needs both the weight and failure load and requires the test result. By comparing their values, it is concluded that the difference between r_1 and r_2 is negligible for our test results.

Figures 4 and 5 depict the variations of K_{ICM} and K_{IICM}, which are conventional critical stress intensity factors or apparent fracture toughness values in the mixed mode condition for mode I and mode II, respectively, for different notch-depth ratios, α,

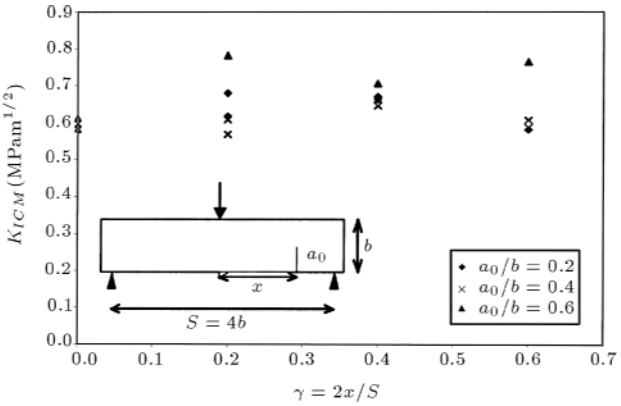

Figure 4. Conventional mode I fracture toughness for different notch configurations.

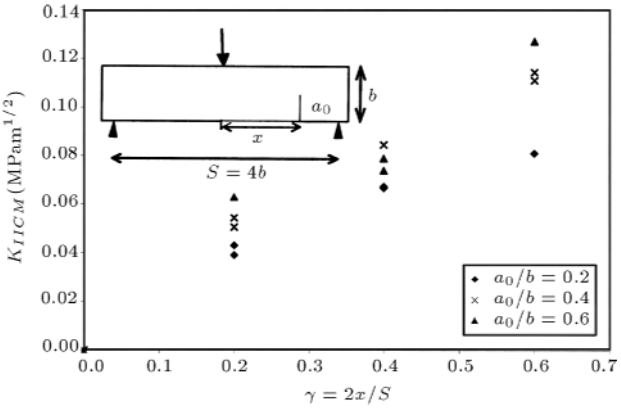

Figure 5. Conventional mode II fracture toughness for different notch configurations.

and offset ratios, γ. It can be observed that for each particular notch-depth ratio, as the offset ratio increases, the value of K_{IICM} increases too. This may be due to the effect of aggregate interlock in the case of a mixed mode fracture; this interlock has little effect on K_{ICM}.

In LEFM condition, a simple interaction relation for the failure locus, based on values of K_I and K_{II}, is proposed [2,13]:

$$\left(\frac{K_{ICM}}{K_{IC}}\right)^2 + \left(\frac{K_{IICM}}{K_{IIC}}\right)^2 = 1, \tag{17}$$

where K_{IC} and K_{IIC} are fracture toughness values for pure mode I and mode II, respectively. However, in concrete, due to the presence of a large Fracture Process Zone (FPZ), LEFM criteria are not suitable. In this study, by using a larger thickness (t = 150 mm), which results in smaller FPZ in comparison to other investigations, the plane strain condition was approximated. To have a better observation, a conventional mixed mode critical stress intensity factor is also calculated:

$$K_C = \sqrt{(K_{ICM})^2 + (K_{IICM})^2}. \tag{18}$$

Table 2. Experimental results of peak load and conventional critical mode I, II stress intensity factors.

Specimen	x (mm)	a_0 (mm)	$P_{\max}$ (kN)	K_{ICM} (MPam$^{1/2}$)	K_{IICM} (MPam$^{1/2}$)	$r_1 = K_{IIP}/K_{IP}$	$r_2 = K_{IICM}/K_{ICM}$
C0001	-	0.0	16.832	-	-	-	-
C0002	-	0.0	15.179	-	-	-	-
C0031	0	30.0	7.191	0.588	0.000	0.0000	0.0000
C0032	0	30.0	7.191	0.588	0.000	0.0000	0.0000
C0061	0	61.2	4.114	0.596	0.000	0.0000	0.0000
C0062	0	61.2	4.114	0.596	0.000	0.0000	0.0000
C0091	0	90.0	2.098	0.581	0.000	0.0000	0.0000
C0092	0	90.0	2.217	0.612	0.000	0.0000	0.0000
C0631	60	30.0	8.571	0.616	0.039	0.0641	0.0633
C0632	60	30.0	9.463	0.679	0.043	0.0641	0.0634
C0661	60	61.3	4.828	0.607	0.054	0.0914	0.0894
C0662	60	61.6	4.471	0.567	0.051	0.0914	0.0892
C0691	60	90.0	3.401	0.781	0.063	0.0831	0.0805
C0692	60	90.0	Failed	-	-	-	-
C1231	120	33.0	11.705	0.665	0.067	0.1012	0.1004
C1232	120	33.0	11.795	0.670	0.067	0.1012	0.1004
C1261	120	61.2	6.926	0.646	0.084	0.1325	0.1308
C1262	120	61.2	6.926	0.646	0.084	0.1325	0.1308
C1291	120	90.0	3.847	0.661	0.074	0.1142	0.1118
C1292	120	90.0	4.114	0.705	0.079	0.1142	0.1119
C1831	180	33.0	14.333	Failed at center	-	-	-
C1832	180	33.0	15.360	0.580	0.081	0.1402	0.1396
C1861	180	60.0	9.765	0.587	0.111	0.1897	0.1886
C1862	180	60.0	10.066	0.605	0.114	0.1897	0.1887
C1891	180	90.0	6.790	0.764	0.127	0.1673	0.1661
C1892	180	90.0	6.790	0.764	0.127	0.1673	0.1661

Figure 6 shows the values of K_C for different notch configurations. It does imply that K_C can be assumed almost a constant. It is worth noting that in the case of $a_0/b = 0.6$, the FPZ is larger with respect to ligament size; therefore, the higher values of K_C seem logical and LEFM is less accurate.

It should be mentioned that the calculated values of conventional mixed mode critical stress intensity factors are lower than those of some other experimental results [5], which is due to the thickness effect. Wollrab et al. [15] have investigated the effect of thickness on the fracture behavior of concrete and have concluded that fracture toughness decreases with increasing specimen thickness, somehow similar to metals [13].

Figure 7 presents the variations of K_{ICM} with K_{IICM}. It can be seen that when K_{IICM} increases, a slight increase is produced in K_{ICM}. Two reasons can be pointed out here:

1. By increasing K_{IICM} values, the aggregate interlock stress will increase, resulting in higher values for K_{ICM};
2. For larger γ, therefore at larger K_{IICM}, due to the presence of some horizontal friction force at the sliding support, the effective bending stress decreases.

Crack Angle

For each specimen, two angles were determined, the first being the initiation angle and the other being the final failure angle, which were calculated based on the

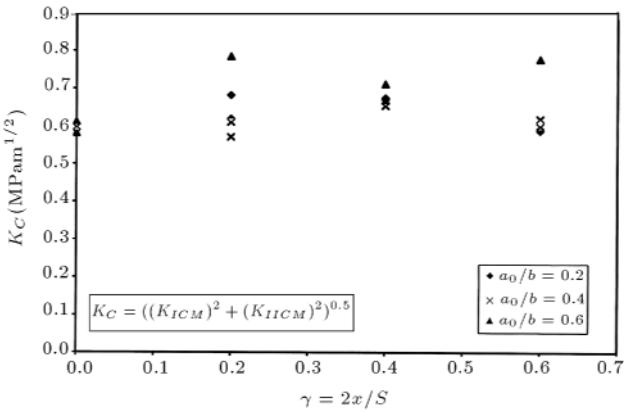

Figure 6. Variation of conventional K_C for different notch configurations.

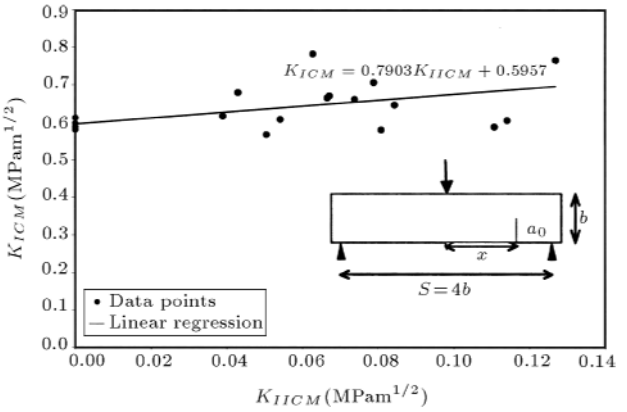

Figure 7. Failure locus for the mixed mode conventional critical stress intensity factors.

intersection point of the crack with the beam's top side. The results are presented in Table 3. Some specimens have shown failures along non-orthogonal planes to the lateral sides of the beam, owing to non-planar deformations at the crack front; therefore, the average angle through the thickness of the beam was considered. Figures 8 and 9 present the results for the crack angles in comparison to the theoretical results based on the maximum principal stress criterion (Equation 4). It is observed that the values agree much better in cases of final failure angles, emphasizing that for the initiation angle, erroneous values may be measured due to the presence of aggregates dispersed throughout the crack front.

Crack Trajectories

Figure 10 shows the crack trajectories for the current investigation. For each specimen, both sides of the beam were considered. To better understand the trends in the nature of the scatter, the following remarks may be considered:

1. The undulations in the crack path, which are not

Figure 8. Measured initiation and final failure angles.

$\gamma = 2x/S$	$\alpha = a_0/b$	Initiation Angle		Final Angle	
0.0	0.2	0	0	0	0
	0.4	0	0	0	0
	0.6	0	0	0	0
0.2	0.2	5	8	8	8
	0.4	10	17	13	10
	0.6	20	-	14	-
0.4	0.2	11	21	11	23
	0.4	13	18	13	8
	0.6	34	30	12	-
0.6	0.2	-	-	-	22
	0.4	22	25	26	19
	0.6	36	31	30	30

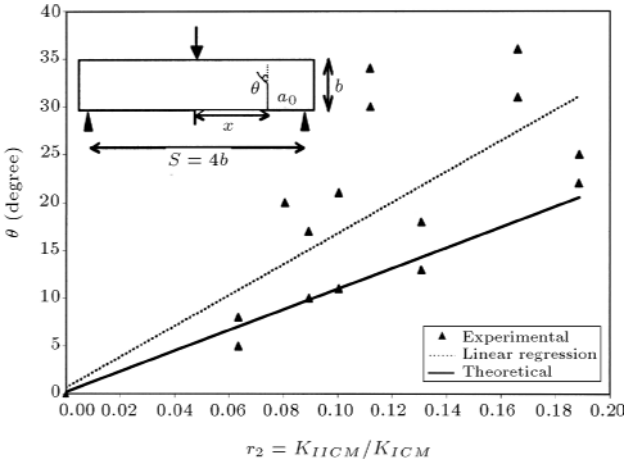

Figure 8. Theoretical prediction and experimental measurements of initiation angle.

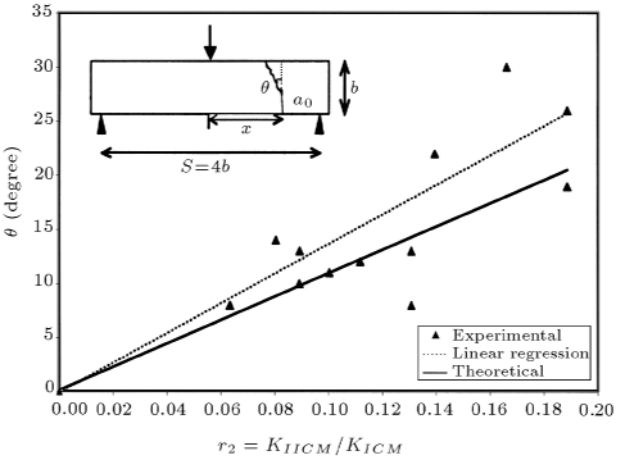

Figure 9. Theoretical prediction and experimental measurements of final failure angle.

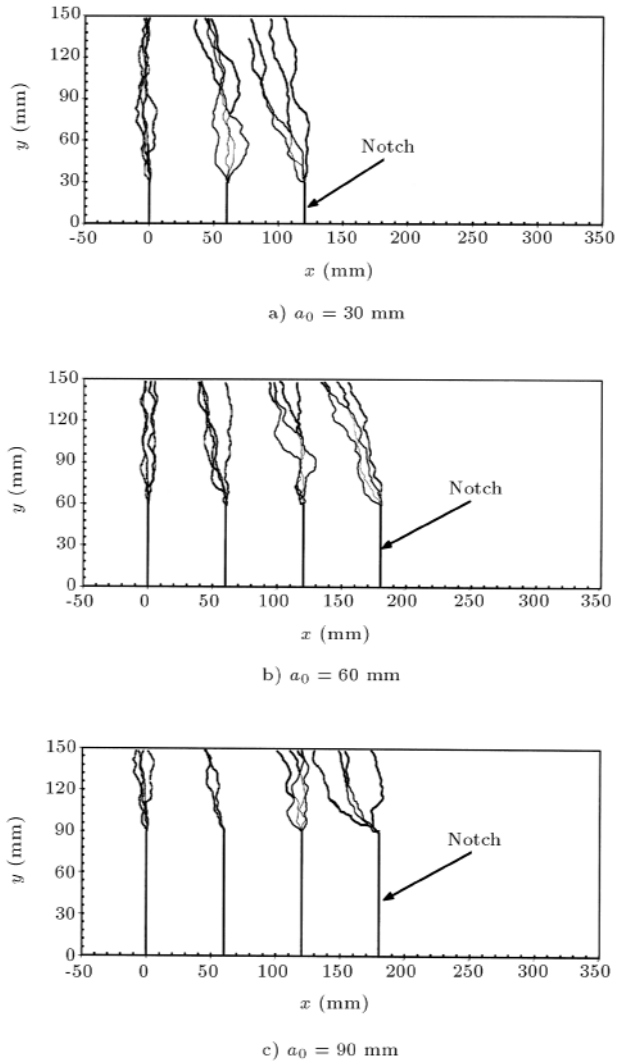

Figure 11. Experimental crack trajectories.

normally observed in metal fracture specimens, are caused by aggregate dispersion in the concrete. For the same reason, a difference of about one coarse aggregate size was observed between the crack paths on the front and back surfaces of each specimen;

2. In the case of lower notch depths, the crack path seems better predictable. This is because in those specimens the ligament size is large enough, compared to maximum aggregate size, for the crack to correct its path, as it is for homogeneous materials.

The crack patterns reveal that by increasing the offset ratio, the final failure angle of the crack increases, which highlights the effect of mode II in fracture.

CONCLUSIONS

The mixed mode fracture of concrete beam specimens, with a relatively large thickness, was investigated. It was observed that the large thickness provides a condition closer to plane strain and improves the accuracy of LEFM criteria. This effect was seen in the total conventional fracture toughness, K_C, value, which was almost independent of notch depth and location. For the effect of weight, separate stress intensity factors are required for large structures. The experimental final failure angles obtained from the fractured specimens are approximately the same as initial angles found from maximum principal stress criterion. Frictional tractions from the aggregate interlock may increase conventional fracture toughness, by increasing the mode II to mode I stress intensity factors ratio.

ACKNOWLEDGMENT

This research has been conducted in the Materials and Structures Laboratory of the Civil Engineering Department at Sharif University of Technology. The authors would like to thank the laboratory personnel for their continued assistance.

REFERENCES

1. Jenq, Y.S. and Shah, S.P. "Features of mechanics of quasi-brittle crack propagation in concrete", *Int. J. of Fracture*, **51**, pp 103-120 (1991).
2. Shah, S.P., Swartz, S.E. and Ouyang, C., *Fracture Mechanics of Concrete*, John Wiley and Sons, New York, USA (1995).
3. Bazant, Z.P. and Planas, J., *Fracture and Size Effect in Concrete and Other Quasibrittle Materials*, CRC Press, Florida, USA (1998).
4. Bazant, Z.P. "Concrete fracture models: Testing and practice", *Engrg. Fracture Mech.*, **69**, pp 165-205 (2002).
5. Jenq, Y.S. and Shah, S.P. "Mixed-mode fracture of concrete", *Int. J. of Fracture*, **38**, pp 123-142 (1988).
6. Swartz, S.E., Lu, L.W., Tang, L.D. and Refai, T.M. "Mode II fracture parameter estimates for concrete from beam specimens", *Experimental Mechanics*, **28**(2), pp 146-153 (1988).
7. Swartz, S.E. and Taha, N.M. "Mixed mode crack propagation and fracture in concrete", *Engrg. Fracture Mech.*, **35**, pp 137-144 (1990).
8. Soroushian, P., Elyamany, H., Tlili, A. and Ostowari, K. "Mixed-mode fracture properties of concrete reinforced wit h low volume fractions of steel and polypropylene fibers", *Cement and Concrete Composites*, **20**, pp 67-78 (1998).
9. Biolzi, L. "Mixed mode fracture in concrete beams", *Engrg. Fracture Mech.*, **35**, pp 187-193 (1990).
10. Guo, Z.K., Kobayashi, A.S. and Hawkins, N.M. "Mixed modes I and II concrete fracture: An experimental analysis", *J. of Applied Mech.*, **61**, pp 815-821 (1994).

11. Galvez, J.C., Elices, M., Guinea, G.V. and Planas, J. "Mixed mode fracture of concrete under proportional and nonproportional loading", *Int. J. of Fracture*, **94**, pp 267-284 (1998).

12. Cendon, D.A., Galvez, J.C. and Planas, J. "Modeling the fracture of concrete under mixed mode loading", *European Congress on Computational Methods in Applied Sci. and Engrg.*, Barcelona, Spain (2000).

13. Broek, D., *Elementary Engineering Fracture Mechanics*, Kluwer Academic Publishers, Dordrecht, The Netherlands (1986).

14. Barsoum, R. "Application of quadratic isoparametric finite elements in linear fracture mechanics", *Int. J. of Fracture*, **10**, pp 603-605 (1974).

15. Wollrab, E., Ouyang, C., Shah, S.P., Hamms, J. and Konig, G. "The effect of specimen thickness on fracture behavior of concrete", *Magazine of Concrete Research*, **48**, pp 117-129 (1996).